Resonant X-ray emission spectroscopy reveals d–d ligand-field states involved in the self-assembly of a square-planar platinum complex

Resonant X-Ray Emission Spectroscopy Reveals d–d Ligand-Field States Involved in the Self-Assembly of a Square-Planar Platinum Complex

Claudio Garino, Erik Gallo, Nikolay Smolentsev, Pieter Glatzel, Roberto Gobetto, Carlo Lamberti, Peter J. Sadler and Luca Salassa

Phys. Chem. Chem. Phys., 2012, **14**, 15278–15281

doi: 10.1039/c2cp42451g

Resonant X-Ray Emission Spectroscopy Reveals d–d Ligand-Field States Involved in the Self-Assembly of a Square-Planar Platinum Complex

Claudio Garino,*[a] Erik Gallo,[b] Nikolay Smolentsev,[bc] Pieter Glatzel,[b] Roberto Gobetto,[a] Carlo Lamberti,[a] Peter J. Sadler[d] and Luca Salassa*[de]

Resonant X-ray Emission Spectroscopy (RXES) is used to characterize the ligand field states of the prototypic self-assembly square-planar complex, [Pt(tpy)Cl]Cl (tpy = 2,2′:6′,2″-terpyridine), and determine the effect of weak metal-metal and π–π interactions on their energy.

Supramolecular assembly promoted by non covalent metal–metal interactions and π–π stacking has been effectively employed to fine-tune the photophysical, photochemical and redox properties of d^8 and d^{10} transition metal complexes, fostering the development of novel materials able to respond to subtle alterations in their chemical microenvironments (e.g. by drastic color and luminescence changes).[1-5] In square-planar platinum(II) complexes with terpyridine ligands, favorable Pt···Pt and π–π intermolecular interactions produce oligomeric structures which have been exploited to detect biomolecules such as glucose[1] and to probe events such as G-quadruplex formation and nuclease activity spectroscopically.[6] Remarkable absorption and emission changes (e.g. luminescence shift to the NIR) are observed in these systems, due to the metal-metal-to-ligand charge transfer transitions (^{3}MMLCT) generated by aggregation of Pt-terpyridine units. Precise knowledge of the structural and electronic effects induced by weak supramolecular interactions on excited states is crucial to control the optical features of self-assembled metal complexes.

NMR[7] and light scattering[8] have been used to obtain structural information on the aggregates of square-planar platinum(II) complexes, while UV-Vis and luminescence spectroscopy[9, 10] have provided insights into the formation of such aggregates by determining energy shifts of d (Pt) → π (ligand) transitions (e.g. Pt → terpyridine). Conversely, and despite their key role in the deactivation of emissive charge-transfer states, d–d ligand field (LF) states remain elusive for their intrinsic nature (Laporte forbidden) and have been insufficiently characterized with conventional techniques, both for isolated metal complexes and their supramolecular derivatives.

In this work, we use resonant X-ray emission spectroscopy (RXES) to investigate d–d LF transitions in supramolecular aggregates formed in solution by self-assembly of a square-planar platinum complex.

RXES is a synchrotron-based hard X-ray technique which offers unique possibilities to measure selectively d–d transitions of metal ions in solids and in solution. This element-selective technique combines (on two-dimensional maps) X-ray absorption near edge structure (XANES) and valence-to-core X-ray emission spectroscopy (XES). While XANES is sensitive to the unoccupied electronic states and to the local geometry of the absorbing atom (*i.e.* Pt), valence-to-core XES probes the occupied density of states (DOS). Briefly, in RXES an incident photon of energy Ω excites a Pt core electron (e.g. 2p, L-edge) to fill a 5d valence state (*i.e.* unoccupied orbital), then relaxation of a valence 5d electron (*i.e.* occupied orbital) occurs with emission of a photon of energy ω and formation of an electronic final state (Scheme 1). The energy transmitted to the sample is the energy transfer, Ω – ω, which corresponds to a charge-neutral excitation within the 5d shell. The experiment yields a two-dimensional intensity distribution that is plotted versus the incident energy Ω and the energy transfer Ω – ω. Importantly, the final state resembles the optical excited states observed in UV-Vis spectroscopy. However, RXES is a second order process with two dipole transitions as compared to one in UV-Vis; this gives access to LF states and make the method ideal to study their properties.[11, 12]

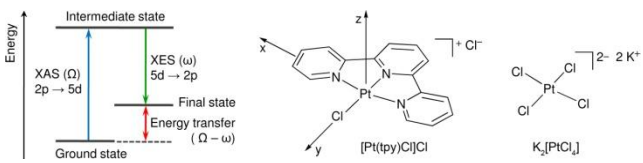

Scheme 1 Simplified energy diagram for RXES at Pt L edge. Structures of [Pt(tpy)Cl]Cl and $K_2[PtCl_4]$.

We report here an unprecedented study aimed at capturing the subtle changes of d–d LF transitions in the supramolecular aggregates of a square-planar Pt^{II} complex. Characterization of these states is crucial to the design of higher-order materials responsive to the environment and displaying outstanding optical features. We choose [Pt(tpy)Cl]Cl (tpy = 2,2′:6′,2″-terpyridine, Scheme 1) as a prototype for studying intermolecular weak Pt···Pt and π–π stacking interactions[13-15] for its well-known ability to give high-order stacked intermolecular aggregates due to its planar structure.[7, 9, 10] Indeed, it was demonstrated by NMR that [Pt(tpy)Cl]Cl self-aggregates in solution forming nanorod-like

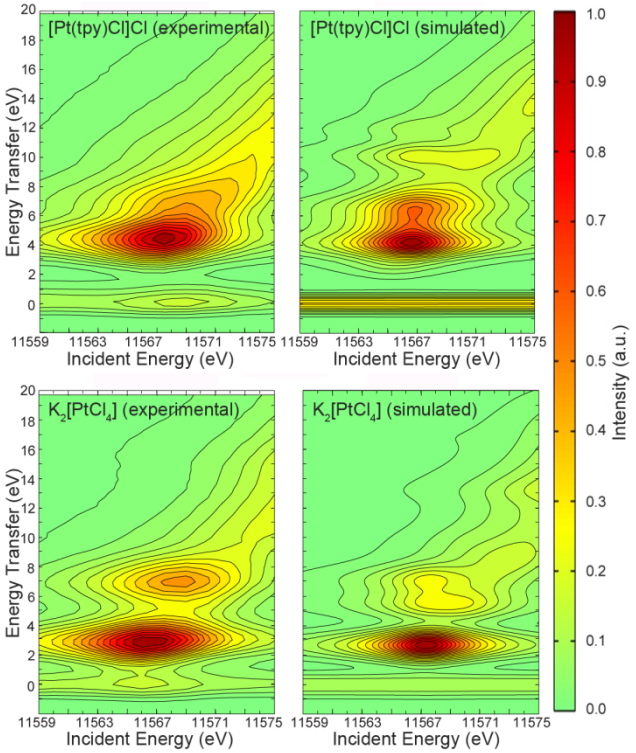

Fig. 1 Contour plots of experimental (left) and simulated (right) Pt-L_3 ($2p_{3/2}$) RXES planes for solid [Pt(tpy)Cl]Cl (top) and solid $K_2[PtCl_4]$ (bottom).

structures (e.g. length of 0.7–2.9 nm, 3–10 molecules, in the 1–25 mM range at 25 ºC).[7]

The complex does not emit in solution owing to the presence of low-lying d–d LF excited states, which deactivate the emissive metal-to-ligand charge-transfer (^{3}MLCT) state.[1] It has been demonstrated that substitution of the Cl ligand with a strong σ-donor ligand increases the energy gap between these states and turns on luminescence, however no direct information on the effect of self-assembly on d–d LF states is available for [Pt(tpy)Cl]Cl and other Pt-tpy derivatives.

Pt-L_3($2p_{3/2}$) RXES planes of the [Pt(tpy)Cl]Cl were collected by scanning both Ω and ω energies for a solid sample (pellet), and in aqueous solution at different concentrations (5, 10, 20, and 40 mM). A pellet of $K_2[PtCl_4]$ was used as a reference for calibrating the range of Pt^{II} transitions in a square-planar complex. The maps were acquired in the region corresponding to the edge peak of the Total Fluorescent Yield (TFY) XANES spectrum (Figure SI1 for [Pt(tpy)Cl]Cl). As reference to obtain the zero value on the energy transfer axis, we used the elastic peak, which is generated by the absorption and decay pathways of equal incident and emitted energy. The experiments were performed on the high brilliance X-ray spectroscopy beamline ID26 at the European Synchrotron Radiation Facility (ESRF).[16, 17] A complete description of the experimental setup, data acquisition procedure and sample preparation is reported in the Supporting Information.

The Pt-L_3 RXES map of [Pt(tpy)Cl]Cl as solid sample (Figure 1, top) shows a major broad peak, whose energy position (centre of gravity) is centered on 11567.7 eV (incident energy) and 5.10 eV (energy transfer). At higher energy transfer values (ca. 7.5 eV)

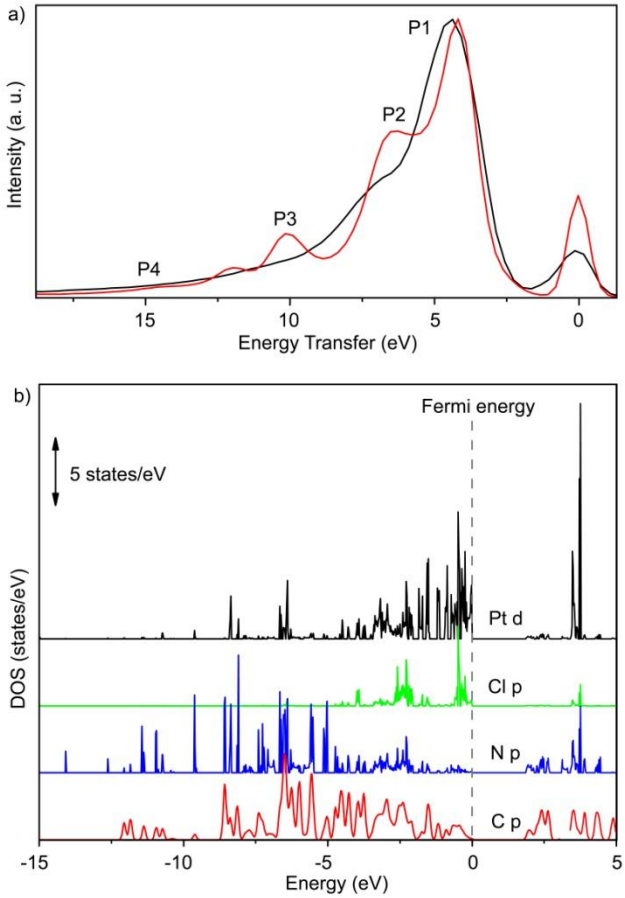

Fig. 2 a) Experimental (black line) and theoretical (red line) Constant Incident Energy (CIE, 11567.7eV) cut of the Pt-L3 ($2p_{3/2}$) RXES plane for solid [Pt(tpy)Cl]Cl. b) Density of states (DOS) obtained using WIEN2k.

a broad tail is observed. The Pt-L_3 RXES map of $K_2[PtCl_4]$ displays two well defined features: a main peak centered at 11566.4 eV (incident energy) and 2.9 eV (energy transfer), and a second peak at 11568.7 eV (incident energy) and 7.0 eV (energy transfer). The centre of gravity energy of the entire multiplet structure is at 11567.5 eV (incident energy) and 4.76 eV (energy transfer). In the reported RXES maps, broadening of the spectral features caused by the lifetime of the Pt 5d core-hole excited state is reduced to the instrumental bandwidth by resonant excitation.[18]

The RXES process is theoretically described by the Kramers-Heisenberg equation.[19, 20] Adequate simulations can be achieved by considering only one-electron transitions (neglecting interference effects and the core hole potential) and adopting computed electronic structures.[19, 21] In particular we used the orbital angular momentum projected density of states (DOS) obtained with the program package WIEN2k,[22, 23] which allows electronic structure calculations of solids at the density functional theory (DFT) level to be performed.

The X-ray structures published by Bailey et al.[9] and by Dickinson[24] were employed as input geometries in the case of [Pt(tpy)Cl]Cl (head-to-tail dimer in unit cell) and $K_2[PtCl_4]$, respectively. The simulated maps for both compounds (Figure 1, right) are in good agreement with the experimental data, as is also confirmed by the constant incident energy (CIE) line plots (Figure 2a for [Pt(tpy)Cl]Cl) extracted (as vertical cuts at

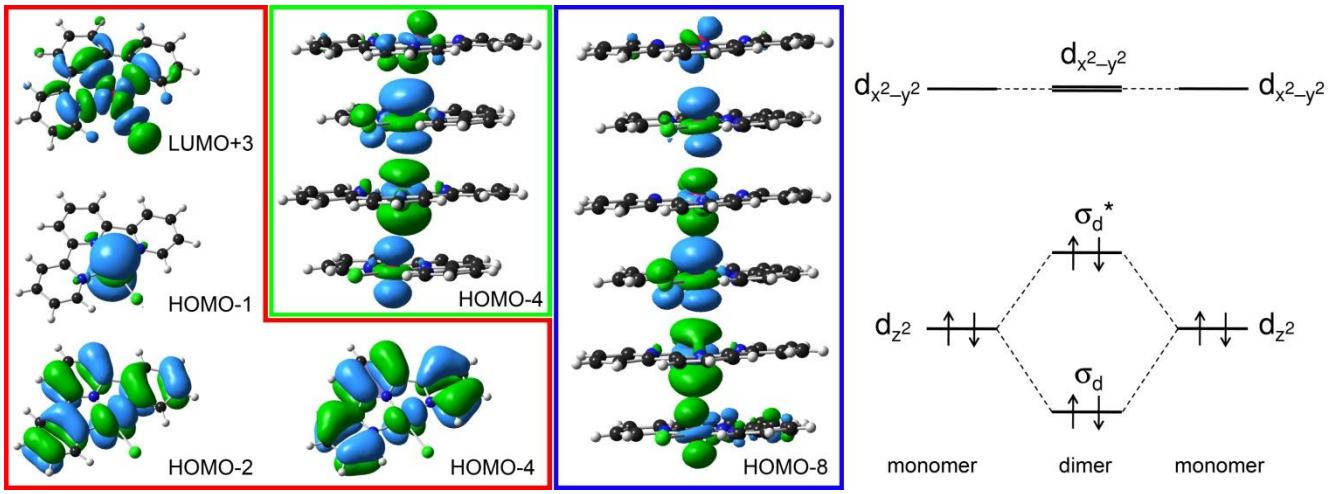

Fig. 3 Selected molecular orbitals (HOMO–4, HOMO–2, HOMO–1, LUMO+3) for $[Pt(tpy)Cl]^+$, together with antibonding combinations (σ_d*) of Pt^{II} filled d_z^2 orbitals for the oligomeric structures $\{[Pt(tpy)Cl]^+\}_4$ (HOMO–4) and $\{[Pt(tpy)Cl]^+\}_6$ (HOMO–8). Simplified MO energy diagram for interaction of two d^8 square-planar units along the metal-metal axis.

Table 1 Center of Gravity[a] Energy for the RXES Spectral Features of [Pt(tpy)(Cl)]Cl and $K_2[PtCl_4]$

		Incident Energy (eV)	Energy Transfer (eV)
[Pt(tpy)(Cl)]Cl	Solid	11567.7	5.10 ± 0.05
	40 mM aq.	11567.8	5.10 ± 0.05
	20 mM aq.	11567.8	5.10 ± 0.05
	10 mM aq.	11567.8	5.50 ± 0.07
	5 mM aq.	11567.8	5.65 ± 0.10
$K_2[PtCl_4]$	Solid	11567.5	4.76 ± 0.03

[a] Defined with the first moment analysis.[25]

11567.7 eV incident energy) from the corresponding experimental and theoretical RXES planes.

Analysis of the density of states (DOS) plotted in Figure 2b indicates that the main peak (P1, 4.3 eV energy transfer) as well as the shoulder (P2, 6.7 eV energy transfer) in the RXES map and CIE cut of [Pt(tpy)Cl]Cl arise from transitions involving Pt-based molecular orbitals (MOs) with prevalent Pt 5d and Cl 3p character (although N and C contributions are also present). The tails at higher energy transfer values (P3 and P4) are attributed to transitions between MOs where the Pt 5d atomic orbitals are mostly mixed with N 2p (and to a lower extent with C 2p) atomic orbitals of the tpy ligand. The presence of four monodentate Cl ligands in $K_2[PtCl_4]$ instead of the chelating tpy is responsible for the disappearance of the high energy tail. Indeed, $K_2[PtCl_4]$ displays two defined peaks due to transitions between MOs with Pt 5d and Cl 3p character.

In aqueous solution, [Pt(tpy)Cl]Cl shows similar RXES features as in the solid state, with a major peak at 11567.8 eV on the incident energy axis (Figure SI2). However, a concentration-dependent shift of the peak along the energy transfer axis is observed with respect to the elastic peak (Table 1).

As for the solid sample, 40 and 20 mM solutions of the complex give an RXES band centered at 5.10 eV (energy transfer), indicating a rather similar extent of supramolecular aggregation in such conditions. Conversely, when the concentration is lowered to 10 mM and 5 mM, the peak moves to higher energy transfer values, reaching 5.50 eV and 5.65 eV respectively. The energy shift is due to changes in the supramolecular structure of [Pt(tpy)Cl]Cl. As observed before, ^{1}H NMR of the complex in D_2O (Figure SI3) shows a concentration dependence; tpy resonances are shifted towards lower frequencies, highlighting variations in the supramolecular structure.[7] In particular, diffusion coefficient NMR measurements demonstrated that aggregates of ca. 10 [Pt(tpy)Cl]Cl units are formed in aqueous solution at 25 mM, while at lower concentrations smaller sized oligomers are present. Our measurements clearly indicate that above 20 mM intermolecular weak interactions induce comparable electronic effects on the Pt 5d orbitals.

To further elucidate these results, we calculated and compared the electronic structures of a series of $[Pt(tpy)Cl]^+$ aggregates using DFT. Head-to-tail $\{[Pt(tpy)Cl]^+\}_n$ oligomers (where n = 2, 4, 6, 8, 10) were packed over one dimension as described in the Supporting Information (Computational details and Figure SI4) and their electronic structures were calculated at the TPSSH/SDD/6-31+G** level in the gas phase.[26-28] The analysis of the MOs of the monomeric $[Pt(tpy)Cl]^+$ shows that the lowest unoccupied MO having significant Pt-d contributions (orbital filled upon the absorption of the incident photon) is LUMO+3. The occupied Pt-based MOs involved in the X-ray emission process to fill the core hole (MOs having Pt-d contributions) are HOMO, HOMO–1, HOMO–2, HOMO–3, and HOMO–4.

LUMO+3 has a strong contribution from the Pt $d_{x^2-y^2}$ orbital, HOMO–2 and HOMO–4 show the character of a Pt d_{yz} orbital, while HOMO, HOMO–1 and HOMO–3 show the contribution of Pt d_{xz}, d_z^2, and d_{xy} orbitals, respectively (Figure 3). Time-dependent DFT (TDDFT) calculations of singlet-singlet transitions actually confirm the contributions of these orbitals in d–d LF optical transitions (Table SI1 and Figure SI5).

Metal–metal interactions occur between filled d orbitals along the axial direction and play a key role in the formation of dimeric, trimeric or oligomeric structures. The orbitals interacting most strongly are those that extend perpendicular to the molecular plane (d_{xz}, d_{yz} and d_z^2). In terms of a simplified MO model, these

orbitals interact in the dimer (or in the oligomers) to split into bonding and antibonding combinations: σ_d and σ_d* for d_z^2 or π_d and π_d* for d_{xz} (and d_{yz}).[29, 30] Conversely, Pt $d_{x^2-y^2}$ orbitals such as in the LUMO+3 do not mix, and hence do not change significantly their energy. This results in a decrease of the gap between the occupied σ_d* and π_d* orbitals of the dimer (or oligomer) and its unoccupied d orbitals. Therefore, d–d LF transitions (e.g. $\sigma_d^* \rightarrow d_{x^2-y^2}$) are less energetic relative to monomer transition ($d_z^2 \rightarrow d_{x^2-y^2}$), supporting the shift of the RXES main band to lower energies upon concentration increase. As an example, Figure 3 reports occupied frontier orbitals for $\{[Pt(tpy)Cl]^+\}_4$ and $\{[Pt(tpy)Cl]^+\}_6$ that arise from antibonding combinations of d_z^2 orbitals. Similar results are also found for higher order aggregates, and are in good agreement with the solid-state DOS calculated by WIEN2k. Although direct comparison with the centre of mass energy of the experimental RXES peak is pointless, the energy gap between frontier molecular orbitals containing d_z^2 and $d_{x^2-y^2}$ components gives a qualitative confirmation of the observed red shift in the RXES signal upon self-assembly. Calculations show that increasing the size from monomer to decamer reduces the HOMO–LUMO gap energy of ca. 2 eV, in qualitative agreement with the 0.5 eV decrease observed experimentally in the peak centre of gravity.

Remarkably, RXES provides direct evidence of the energy shift in the d–d LF transitions caused by metal–metal and π–π stacking interactions. DFT electronic structure analysis not only supports the experimental results, but also gives specific insights in the electronic effects of self-assembly. The d_z^2 orbital mixing is key for lowering the energy of d–d LF transitions in Pt-tpy systems, strongly influencing their photophysical properties. However, such interactions among d_z^2 orbitals do not stabilize aggregates, and other forces are likely to play a more relevant role (e.g. coulomb and π–π interactions). The $d_{x^2-y^2}$ orbitals are oriented towards the Pt–ligand bonds and remain substantially unaffected by self-assembly. Interestingly, this finding also helps to rationalize why substitution of a Cl ligand significantly changes the optical properties (increased energy of the LUMO) in Pt-tpy derivatives and suggests, at the same time, that favoring the formation of supramolecular interactions in the plane of the ligands will allow full control of the d–d states to be achieved by directly affecting the $d_{x^2-y^2}$ orbital energy.

More extended studies are necessary to fully explore the potential of RXES in the study of supramolecular chemistry, however, as demonstrated for the first time in this study, the technique can be used to characterize spectroscopically silent states in high-order systems. Hence, RXES can be exploited to guide the design and synthesis of functional supramolecular architectures based on transition metal complexes.

Acknowledgements

The authors acknowledge the European Synchrotron Radiation Facility (ESRF CH3108). L.S. was supported by ERC BIOINCMED (grant no. 247450 to P.J.S.) and the MICINN of Spain with the Ramón y Cajal Fellowship RYC-2011-07787.

Notes and references

[a] *Department of Chemistry and NIS Centre of Excellence, University of Turin, Via P. Giuria 7, 10125 Turin, Italy. Fax: +39 011 6707855; Tel: +39 011 6707946; E-mail: claudio.garino@unito.it*
[b] *European Synchrotron Radiation Facility (ESRF), Rue Jules Horowitz 6, 38043 Grenoble, France.*
[c] *Research Center for Nanoscale Structure of Matter, Southern Federal University, Str. Sorge 5, 344090 Rostov-on-Don, Russia.*
[d] *Department of Chemistry University of Warwick, Gibbet Hill Rd, Coventry CV4 7AL, UK. Fax: +34 943 005301; Tel: +34 943 005323.*
[e] *CIC biomaGUNE, Paseo Miramón 182, 20009 Donostia– San Sebastian, Spain; E-mail: lsalassa@cicbiomagune.es*

† Electronic Supplementary Information (ESI) available: details on materials and methods, sample preparation, data acquisition, data analysis, and computational method; TFY XANES spectrum of [Pt(tpy)(Cl)]Cl in the solid state; experimental Pt-L_3 ($2p_{3/2}$) RXES planes in aqueous solution and ^{1}H NMR spectra in D_2O of [Pt(tpy)(Cl)]Cl at different concentrations; calculated singlet excited-states transitions for $[Pt(tpy)(Cl)]^+$ in water, experimental UV-Vis absorption spectrum for an aqueous solution of [Pt(tpy)Cl]Cl and calculated singlet excited state transitions, fit of the elastic peak in the CIE cut (11567 eV) of the Pt-L_3 ($2p_{3/2}$) RXES plane for [Pt(tpy)Cl]Cl in aqueous solutions. See DOI: 10.1039/b000000x/

1. V. W.-W. Yam and K. M.-C. Wong, *Chem. Commun.*, 2011, **47**, 11579-11592.
2. A. J. Goshe, I. M. Steele and B. Bosnich, *J. Am. Chem. Soc.*, 2003, **125**, 444-451.
3. D. R. McMillin and J. J. Moore, *Coord. Chem. Rev.*, 2002, **229**, 113-121.
4. V. Adamovich, J. Brooks, A. Tamayo, A. M. Alexander, P. I. Djurovich, B. W. D'Andrade, C. Adachi, S. R. Forrest and M. E. Thompson, *New J. Chem.*, 2002, **26**, 1171-1178.
5. V. W. W. Yam, K. M. C. Wong and N. Y. Zhu, *Angew. Chem. Int. Ed.*, 2003, **42**, 1400-1403.
6. C. Yu, K. H.-Y. Chan, K. M.-C. Wong and V. W.-W. Yam, *Chem. Commun.*, 2009, 3756-3758.
7. A. M. Krause-Heuer, N. J. Wheate, W. S. Price and J. Aldrich-Wright, *Chem. Commun.*, 2009, 1210-1212.
8. G. Arena, L. M. Scolaro, R. F. Pasternack and R. Romeo, *Inorg. Chem.*, 1995, **34**, 2994-3002.
9. J. A. Bailey, M. G. Hill, R. E. Marsh, V. M. Miskowski, W. P. Schaefer and H. B. Gray, *Inorg. Chem.*, 1995, **34**, 4591-4599.
10. H. K. Yip, L. K. Cheng, K. K. Cheung and C. M. Che, *J. Chem. Soc., Dalton Trans.*, 1993, 2933-2938.
11. U. Bergmann and P. Glatzel, *Photosynth. Res.*, 2009, **102**, 255-266.
12. P. Glatzel and U. Bergmann, *Coord. Chem. Rev.*, 2005, **249**, 65-95.
13. G. Lowe, A. S. Droz, T. Vilaivan, G. W. Weaver, J. J. Park, J. M. Pratt, L. Tweedale and L. R. Kelland, *J. Med. Chem.*, 1999, **42**, 3167-3174.
14. S. J. Lippard, *Acc. Chem. Res.*, 1978, **11**, 211-217.
15. E. M. A. Ratilla, H. M. Brothers and N. M. Kostic, *J. Am. Chem. Soc.*, 1987, **109**, 4592-4599.
16. C. Gauthier, V. A. Sole, R. Signorato, J. Goulon and E. Moguiline, *J. Synchrot. Radiat.*, 1999, **6**, 164-166.
17. P. Glatzel, J. Singh, K. O. Kvashnina and J. A. van Bokhoven, *J. Am. Chem. Soc.*, 2010, **132**, 2555-2557.
18. N. Smolentsev, M. Sikora, A. V. Soldatov, K. O. Kvashnina and P. Glatzel, *Phys. Rev. B*, 2011, **84**.
19. A. Kotani and S. Shin, *Rev. Mod. Phys.*, 2001, **73**, 203-246.
20. F. Gel'mukhanov and H. Agren, *Phys. Rep.-Rev. Sec. Phys. Lett.*, 1999, **312**, 87-330.
21. J. Jimenez-Mier, J. van Ek, D. L. Ederer, T. A. Callcott, J. J. Jia, J. Carlisle, L. Terminello, A. Asfaw and R. C. Perera, *Phys. Rev. B*, 1999, **59**, 2649-2658.
22. P. Blaha, K. Schwarz, G. K. H. Madsen, D. Kvasnicka and J. Luitz, *WIEN2k: An Augmented Plane Wave + Local Orbitals Program for Calculating Crystal Properties*, (2001) Karlheinz Schwarz Technische Universität, Wien, Austria.
23. K. Schwarz, P. Blaha and S. B. Trickey, *Mol. Phys.*, 2010, **108**, 3147-3166.
24. R. G. Dickinson, *J. Am. Chem. Soc.*, 1922, **44**, 2404-2411.

25. P. Glatzel, U. Bergmann, J. Yano, H. Visser, J. H. Robblee, W. W. Gu, F. M. F. de Groot, G. Christou, V. L. Pecoraro, S. P. Cramer and V. K. Yachandra, *J. Am. Chem. Soc.*, 2004, **126**, 9946-9959.
26. J. Tao, J. P. Perdew, V. N. Staroverov and G. E. Scuseria, *Phys. Rev. Lett.*, 2003, **91**, 146401.
27. P. Fuentealba, H. Preuss, H. Stoll and L. Von Szentpály, *Chem. Phys. Lett.*, 1982, **89**, 418-422.
28. R. Ditchfield, W. J. Hehre and J. A. Pople, *J. Chem. Phys.*, 1971, **54**, 724-728.
29. K. Krogmann, *Angew. Chem. Int. Ed.*, 1969, **8**, 35-42.
30. A. Dedieu, *Chem. Rev.*, 2000, **100**, 543-600.